ACS Sustainable Chemistry & Engineering

pubs.acs.org/journal/ascecg

Research Article

Butene-Rich Alkene Formation from 2,3-Butanediol through Dioxolane Intermediates

Michael J. Cordon,* Meijun Li, Xiaokun Yang, Peter G. N. Neate, Kinga A. Unocic, Zhenglong Li, Cameron M. Moore, and Andrew D. Sutton*

Cite This: https://doi.org/10.1021/acssuschemeng.4c01155

Read Online

ACCESS | Metrics & More | Article Recommendations | Supporting Information

ABSTRACT: The cost-effective production of sustainable aviation fuels (SAF) remains a major challenge within the energy sector. One approach to address this is the fermentation of biomass feedstocks into oxygenates followed by catalytic conversion to alkenes or other oligomerization precursors. 2,3-Butanediol (BDO) is a promising fermentation product due to its four-carbon nature, its decreased microorganism toxicity and associated higher maximum fermentation titers relative to other alcohols and oxygenates, and its capacity to be readily converted into butene isomers and longer chain alkenes. BDO conversion is currently constrained by separation challenges for BDO isolation due to its high boiling point and hydrophilicity. This work expands upon previous BDO reactive separation via dioxolane formation over a solid acid catalyst by investigating the conversion of dioxolane into alkene mixtures. Dioxolanes can be formed from a range of aldehydes and subsequently converted over a Cu/ZSM-5 catalyst (448−523 K) via an ether cleavage, hydrogenation, and dehydration reaction network to form alkene-rich product mixtures (96% C_{3+} alkene yield, 523 K). This selectivity is greater than that of direct BDO conversion to alkenes over an identical catalyst (89%, 523 K). C_{3+} alkene selectivity is maximized between 498 and 523 K at complete dioxolane conversion without significant alkene hydrogenation to alkanes. The alkene product distributions can be tailored via aldehyde selection during dioxolane formation and the dioxolane conversion reaction temperature. Alkene mixtures from dioxolane conversion predominantly reflect the carbon chain length and stereochemistry of BDO and the initial aldehyde at or below 498 K, yet higher reaction temperatures yield alkene mixtures of similar carbon chain distributions, regardless of initial aldehyde selection. Deactivation of the Cu/ZSM-5 catalyst occurs for multiple steps of the overall reaction network but can be minimized by facilitating the complete dioxolane-to-alkene reaction network at temperatures of at least 498 K.

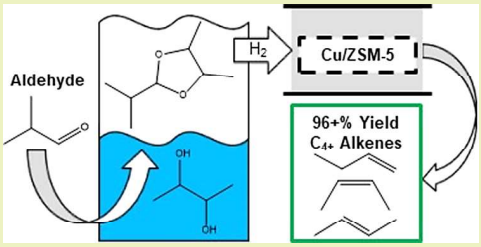

KEYWORDS:

INTRODUCTION

The generation of renewable and sustainable fuels remains a key scientific priority, requiring improved processes for renewable feedstock generation and conversion to liquid fuels. This is especially key for aviation and marine transportation which are difficult to electrify and will require the continued use of energy-dense liquid fuel for the foreseeable future.[1] Biomass fermentation has long been identified as a key pathway for generating alcohols and other oxygenated feedstocks for downstream fuel generation. Ethanol has been classically investigated as a large-scale fermentation product and can be upgraded to middle distillate fuels via alkene formation and subsequent oligomerization and hydrotreating. However, the use of C_1 and C_2 feedstocks is often hindered either by the formation of intermediates such as ethene which are common coke precursors during oligomerization[2] or by difficulties associated with initial C−C bond formation between C_1 monomers such as CO_2.[3] These difficulties could be avoided by tailoring fermentation conditions to generate longer carbon chain alcohols, which can then be converted into C_{3+} alkenes as key fuel production intermediates.

2,3-Butanediol (BDO) has been identified as a potential key renewable feedstock for alkene formation and eventual fuel production. BDO fermentation can be accomplished at higher

Received: February 7, 2024
Revised: April 24, 2024
Accepted: April 25, 2024

titers (>150 g L^{-1}[4,5]) than ethanol or other alcohols due to lower microorganism toxicity, and BDO's four carbon backbone mitigates potential complications associated with the initial C−C bond formation steps of shorter carbon chain compounds. As such, BDO has potential as a fermentation-derived feedstock for upgrading to fuels and chemical production. Although it is not currently economically viable, BDO production, isolation, and utilization are ongoing research areas for future applicability.[6,7] Catalytic upgrading strategies of aqueous BDO solutions can suffer from relatively low BDO reactivities, low BDO concentrations limited by fermentation titers, and high heating costs to vaporize BDO-containing aqueous streams.[6,8] Further, direct BDO upgrading within fermentation broths requires removing a range of cations and other nutrient-derived species to avoid catalyst poisoning.[8] Gas-phase BDO conversion over a bifunctional Cu/ZSM-5 catalyst yields C_{3+} alkene yields above 92% (523 K, 0.2 mL h^{-1} liquid BDO in 30 cm^3 h^{-1} H_2, 1.0 h^{-1} WHSV) via sequential dehydration steps and selective hydrogenation,[9] yet this reaction pathway yields 1,3-butadiene as the key intermediate, a compound that reportedly leads to increased coke formation.[10,11] Further, this pathway utilizes a pure BDO reactant feed, requiring BDO isolation and purification from aqueous solutions. This process is complicated by BDO's high boiling point (177 °C) relative to water and its high water miscibility,[12] making traditional separation methods such as distillation prohibitively expensive due to the necessity of vaporizing large water quantities. Additional separation technologies such as membrane separation,[13] pervaporation,[14] and solvent extraction[15,16] are currently being explored for BDO isolation from fermentation broth, yet the current state of technology must continue to overcome significant technical and economic limitations to increase the industrial viability.

Another BDO separation technique is reactive separation via dioxolane formation, avoiding aqueous-phase upgrading concerns. BDO or another diol can be condensed with a carbonyl-containing compound such as an aldehyde to generate a highly hydrophobic dioxolane, which readily phase separates from aqueous solutions. Dioxolanes can be formed from a range of polyols (e.g., 2,3-butanediol, 1,2-propanediol, ethylene glycol,[17] propylene glycol,[18] glycerol,[19] 3,4-hexanediol, 4,5-octanediol[20]), yet dioxolanes generated from BDO have been obtained at significantly higher yields relative to shorter chain diols.[17] Traditionally, dioxolanes and dioxanes have been widely used for protecting functional groups such as aldehydes or ketones to later recover via hydrolysis,[21] yet dioxolanes themselves have been explored for a wide variety of uses including fungicides and herbicides,[22,23] pharmaceuticals and fragrances,[24] polymers,[25,26] Li-ion battery electrolytes,[27,28] or as a tailored organic solvent.[29,30] Recently, dioxolanes have also been investigated as renewably sourced fuel additives which can increase a fuel's cetane number and density while decreasing its freezing point, viscosity, and soot formation.[31,32] However, isolated dioxolanes could also be directly converted into BDO- and aldehyde-derived molecules including methyl ethyl ketone (MEK), 2-methylpropanal, the parent aldehyde, and associated alcohols which can then be converted into C_{3+} alkene mixtures.[33]

Here, we investigate this expanded application of dioxolane compounds for isolating BDO from the fermentation broth and subsequently generating C_{4+} alkenes. Renewably sourced C_{4+} alkenes are key precursors for renewable fuel generation from fermentation products and are the primary objective of other alcohol conversion technologies including ethanol.[1,34] Dioxolanes are synthesized from BDO and a range of C_2−C_8 aldehydes prior to converting them into C_{4+} alkene mixtures. Dioxolane conversion occurs over a bifunctional Cu/ZSM-5 catalyst previously identified for its catalytic functionality for gas-phase BDO-to-alkene conversion, adding to a growing literature on the development for bifunctional or multifunctional catalysts for sustainable catalysis applications.[35−37] Alkene product compositions are investigated as a function of the reaction temperature and dioxolane composition, the latter of which is controlled by the choice of aldehyde when synthesizing the dioxolane. The wider scale application of dioxolanes for renewable fuel generation is investigated using aldehydes derived from renewable sources (e.g., acetaldehyde from ethanol, furfural, MEK from BDO) to identify potential advantages in the BDO-derived alkene formation process.

RESULTS AND DISCUSSION

To recover BDO from aqueous-phase solutions, aldehydes were introduced over Amberlyst-15 to BDO-rich aqueous solutions (313 K, 6 h, 1.5:1 aldehyde:BDO molar equivalent, >95% yield) to generate dioxolanes as previously published.[31] Scheme 1 depicts a generalized dioxolane formation reaction

Scheme 1. Proposed Reaction Pathway for Generalized Dioxolane Formation via Condensation Reactions from BDO and an Aldehyde[a]

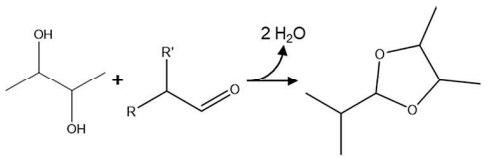

[a]This reaction pathway is known to be catalyzed over Brønsted acid sites such as those found on Amberlyst-15 and is adapted from the previous literature.[31] In this work, R is either a H or a C_2−C_6 linear alkyl chain, and R' is either a H or ethyl group.

adapted from previous literature[31] where aldehyde-derived dioxolanes are known to form over the Brønsted acid sites of Amberlyst-15 (5.1 mmol g^{-1} H^+ density[38]). While dioxolanes can be formed directly from fermentation broth, aldehyde-rich solutions were utilized here for the sake of simplicity. Table 1 lists the dioxolanes synthesized in this work and their corresponding C_2−C_8 aldehyde parents. As the reaction occurs, a separate organic phase forms containing only the dioxolane and residual unreacted aldehyde. Once complete, the organic solutions were decanted and used without additional purification. Mass spectra (Supplementary Figure S1) and NMR spectra (Figure S2) collected of the formed organic phases indicate the presence of three distinct dioxolane diastereomers as previously reported[17,31] and corroborate gas chromatography spectra obtained with a flame ionization detector (GC-FID). Small concentrations of the parent aldehyde are also observed with minimal water uptakes due to low dioxolane-water miscibilities (<40 mg L^{-1}).[31,39] When utilizing short carbon chain aldehydes such as acetaldehyde, a postreaction water addition step is necessary to facilitate the organic and aqueous phase separation. Overall, the formation of dioxolanes from BDO and an aldehyde is a reactive separation technique for removing BDO from aqueous solutions to form a relatively pure reactant mixture.

https://doi.org/10.1021/acssuschemeng.4c01155
ACS Sustainable Chem. Eng. XXXX, XXX, XXX−XXX

Table 1. Dioxolane Reactants Synthesized and Investigated in This Work Were from the Reaction of BDO and Various Aldehydes over Amberlyst-15

Dioxolane Number	IUPAC Name	Aldehyde Reagent	Chemical Structure
1	2,4,5-trimethyl-1,3-dioxolane	Acetaldehyde	
2	4,5-dimethyl-2-propyl-1,3-dioxolane	Butyraldehyde	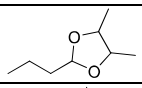
3	4,5-dimethyl-2-(propan-3-yl)-1,3-dioxolane	Isobutyraldehyde	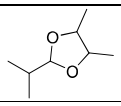
4	4,5-dimethyl-2-pentyl-1,3-dioxolane	Hexaldehyde	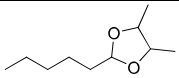
5	4,5-dimethyl-2-(pentan-3-yl)-1,3-dioxolane	2-Ethylbutanal	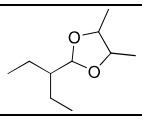
6	4,5-dimethyl-2-heptyl-1,3-dioxolane	Octaldehyde	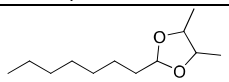
7	2-(heptan-3-yl)-4,5-dimethyl-1,3-dioxolane	2-Ethylhexanal	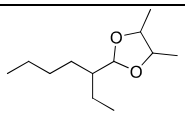

To establish dioxolanes as effective BDO synthons, the conversion of dioxolane to C_{3+} alkenes should be compared with direct BDO conversion. Cu/ZSM-5 has been shown to be an effective catalyst for BDO conversion to C_{3+} alkenes[9] and could also be useful for catalyzing dioxolane conversion to similar products. Cu/ZSM-5 materials were synthesized by Cu incorporation onto a commercial MFI zeolite (Si/Al = 140) via ammonia deposition to generate high Cu loadings (~9−13 wt %). Table 2 lists the key catalyst properties for Cu/ZSM-5 and the key control samples. Both XRD patterns (Figure S3) and micropore volumes derived from N_2 adsorption isotherms (77 K, Figure S4) indicate that the MFI topology is maintained throughout the synthesis process (Table 2). Notably, XRD patterns do not show significant peaks for CuO_x nanoparticles (Figure S3C), indicating that CuO_x nanoparticles are typically small (<3 nm). Micropore volumes decrease after Cu incorporation onto MFI supports (~10 and 30% for H-ZSM-5 and Si-MFI, respectively), yet H-ZSM-5 and Si-MFI materials treated to the ammonia deposition conditions without Cu show negligible micropore volume losses from the basic treatment (pH 9, <10% micropore volume loss). This indicates that some Cu species are occluded within the zeolitic micropores or at the micropore openings, lowering the micropore volume accessible to N_2. This is expected for high Cu loadings such as those present here (~9−13 wt %, Table 2).

Table 2. Micropore Volumes, Elemental Compositions, and Cu Dispersions of the Zeolite Materials Studied Here

sample	V_{ads} (N_2, 77 K)[a] ($cm^3\ g^{-1}$)	Al wt %[b]	Cu wt %[b]	Bronsted acid site density (10^4 mol g^{-1})[d]	Cu dispersion[e]
Cu/ZSM-5	0.128	0.28	9.0	0.45	30.5%
ZSM-5	0.142	0.33		1.17	
Cu/Si-MFI	0.115	n.d.[c]	13.8	0.12	30.8%
Si-MFI	0.152	0.028			

[a]N_2 volumes at the end of the micropore filling transition. [b]Measured via ICP-OES. [c]Not determined. [d]Determined from NH_3 TPD measurements assuming monomolecular NH_3 adsorption. [e]Determined from H_2 TPR experiments after N_2O exposure.

Al Brønsted acid site densities on Cu-free H-ZSM-5, Cu/ZSM-5, and Cu/Si-MFI samples were evaluated using NH_3 TPD and are listed in Table 2. Water fractionation contributions to the m/z = 17 trace were accounted for on all samples. The NH_3 TPD profile collected from H-ZSM-5 (Figure S5) displays a single peak centered at ~645 K reflecting NH_3 desorption from Al Brønsted acid sites.[40,41] Quantification of this peak assuming monomolecular NH_3 adsorption indicates that 92% of total Al sites are Brønsted acidic, matching previously published observations on similar commercial samples.[42] The NH_3 desorption profile of Cu/ZSM-5 shows two peaks where with the higher temperature desorption peak centered at ~560 and 700 K, reflecting NH_3 desorption from Cu species and residual Brønsted acid sites, respectively. Quantifying the higher temperature desorption peak yields ~37% Brønsted acid sites per total Al content where the decrease in NH_3 peak area is caused by Cu exchange onto a subset of the Brønsted acid sites which do not adsorb NH_3 as strongly. Notably, not all of the Brønsted acid sites have been exchanged by Cu ions. A similar desorption profile is observed for Cu/Si-MFI with a much less pronounced second peak centered at ~700 K, reflecting the ~10× lower Al content between the Si-MFI and H-ZSM-5 parent materials. For the remaining Brønsted acid sites on both Cu/ZSM-5 and Cu/Si-MFI materials, the NH_3 desorption peaks shift to significantly higher temperatures around 700 K. The ~55 K shift in NH_3 desorption peak center between Brønsted acid sites on H-ZSM-5 and Cu/ZSM-5 is not caused by interactions with Cu cations which simply decrease high temperature NH_3

https://doi.org/10.1021/acssuschemeng.4c01155
ACS Sustainable Chem. Eng. XXXX, XXX, XXX−XXX

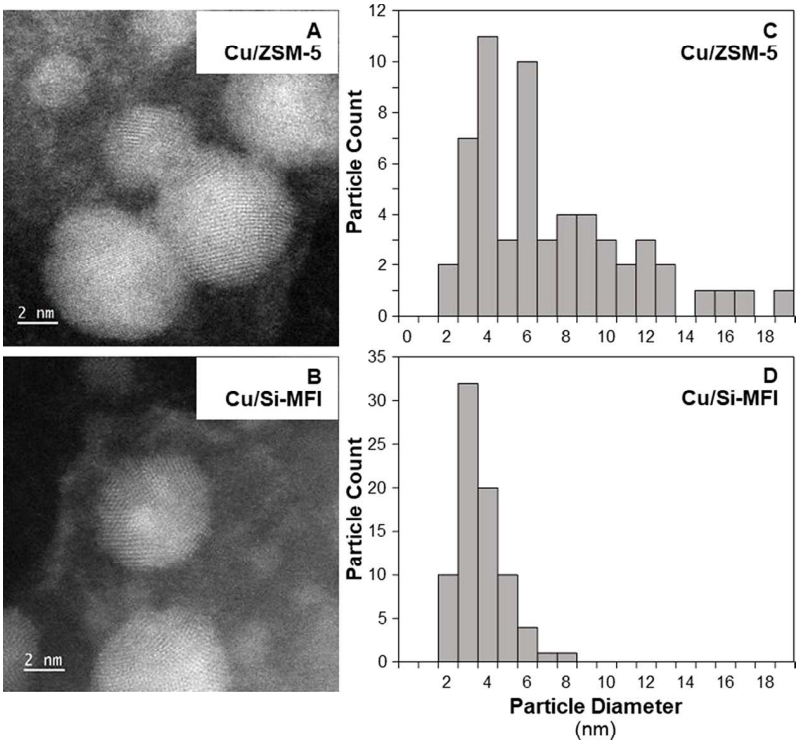

Figure 1. Representative HAADF-STEM images (A,B) and nanoparticle distributions (C,D) measured on Cu/ZSM-5 and Cu/Si-MFI zeolites. Additional HAADF-STEM images are presented in Figure S6.

desorption peak areas[43] but likely reflects an increased NH_3 diffusion path length tortuosity out of the zeolitic micropores with additional readsorption and desorption events.[44,45] Changes in diffusion pathlengths could be caused by Cu sites occluded within zeolitic voids and are evidenced by 10−30% decreases in micropore volume after Cu incorporation procedures.

Bulk Cu distributions were investigated by using HAADF-STEM images and H_2 TPR comparisons from before and after N_2O titration. Figure 1 shows HAADF-STEM images of Cu/ZSM-5 and Cu/Si-MFI (Figure 1A,B, additional images in Figure S6) and associated Cu nanoparticle size distributions (Figure 1C,D). The presence of Cu nanoparticles greater than 3 nm in diameter is observed on both samples, and these nanoparticles are too large to be occluded within the zeolitic micropores of MFI (~0.55 nm diameter). Surface Cu distributions were evaluated by quantifying MS peaks obtained during H_2 TPR both before and after N_2O exposure to the Cu-loaded samples (Figure S7). Since N_2O exposure has been reported to oxidize only surface Cu species[46] due to limited oxygen migration into metallic Cu nanoparticles at 363 K, H_2 TPR measurements taken before and after N_2O exposure correlate with total reducible Cu and only surface Cu sites on Cu nanoparticles, respectively. H_2 TPR measurements indicate that 31 and 30% of Cu sites on Cu/ZSM-5 and Cu/Si-MFI respectively are accessible to oxidation via N_2O. Calculated Cu dispersions then indicate average Cu nanoparticle diameters of 3.7 and 3.6 nm, respectively, further corroborating the bulk Cu distribution measurements observed from HAADF-STEM images despite the lack of XRD peaks reflecting larger CuO_x nanoparticles on either the Cu/ZSM-5 or Cu/Si-MFI materials. This could reflect differences in the CuO_x nanoparticle sizes before and after reduction. Taken together, Cu active site distributions reflect a range of mostly 2−10 nm CuO_x nanoparticles, with ~30% of Cu sites accessible on nanoparticle surfaces as potential catalytically relevant active sites. These materials were then studied for catalyzing the dioxolane-to-alkenes reaction pathway.

Using **3** as a representative dioxolane reactant, Figure 2 depicts transient dioxolane conversion (473 K) and key product yields over Cu/ZSM-5, Cu/Si-MFI, H-ZSM-5, and a physical mixture of Cu/Si-MFI and HZSM-5, while Figure 3 depicts the product distributions measured over these four catalysts at ~3 h time-on-stream as representative product distribution, allowing for easier comparison of product compositions (see Figure S8 for more detailed product selectivity profiles). Cu/Si-MFI and H-ZSM-5 were investigated as control samples to isolate the roles of Cu and Al, respectively. A physical mixture of Cu/Si-MFI and H-ZSM-5 was also investigated for comparison with Cu/ZSM-5, where the physical mixture maintains similar bulk Cu and Al active site densities without potential proximal Cu and Al species. Key products observed from dioxolane conversion include MEK, isobutyraldehyde, butanol, butene isomers, and other alkenes. Each catalyst exhibits transient deactivation, yet dioxolane conversions are significantly and consistently the highest over Cu/ZSM-5. Dioxolane conversions are negligible over Cu-free Si-MFI (not shown) and Al-free Cu/Si-MFI (Figure 2C) while Cu-free H-ZSM-5 yields high initial dioxolane conversions that rapidly deactivate (Figure 2D). This indicates the catalytic significance of Al sites for the initial step(s) of the dioxolane-to-alkenes pathway.

As seen in Figures 2D and 3, product distributions collected over H-ZSM-5 show MEK and isobutyraldehyde as the primary two products from the conversion of **3** over H-ZSM-5, indicating that the Al sites catalyze successive ether cleavage reactions of the dioxolane 5-member ring to return the parent aldehyde and MEK, a BDO-derivative.[8,47] Ether

https://doi.org/10.1021/acssuschemeng.4c01155
ACS Sustainable Chem. Eng. XXXX, XXX, XXX−XXX

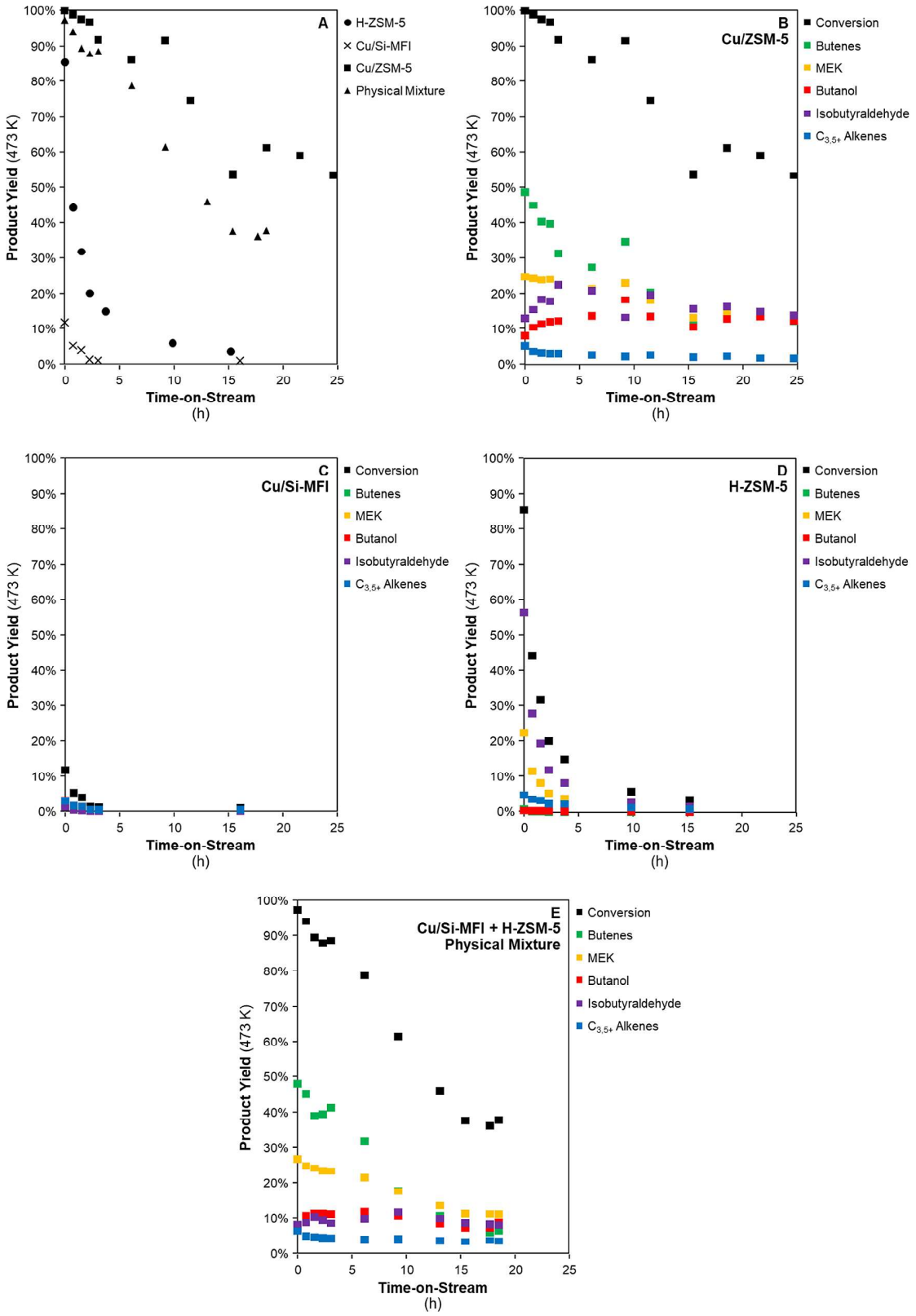

Figure 2. (A) Transient conversions of **3** over the catalysts investigated here and transient conversions and key product distributions measured over (B) Cu/ZSM-5, (C) Cu/Si-MFI, (D) H-ZSM-5, and (E) the physical mixture of Cu/Si-MFI and H-ZSM-5 (5 kPa dioxolane in 96 kPa H_2, 473 K, 2.38 h^{-1} w8 hly space velocity (WHSV) over Cu/ZSM-5, Cu/Si-MFI, and H-ZSM-5 or 1.18 h^{-1} over the physical mixture). The catalyst loading of the physical mixture of Cu/Si-MFI and H-ZSM-5 aimed to match the Cu and Al loadings of Cu/ZSM-5.

cleavage is typically facilitated via protonation as the first mechanistic step, so this reaction is then reasonably assignable to Brønsted acidic Al sites, which can protonate a dioxolane ether. The lack of dioxolane conversion over Cu/Si-MFI is due

https://doi.org/10.1021/acssuschemeng.4c01155
ACS Sustainable Chem. Eng. XXXX, XXX, XXX−XXX

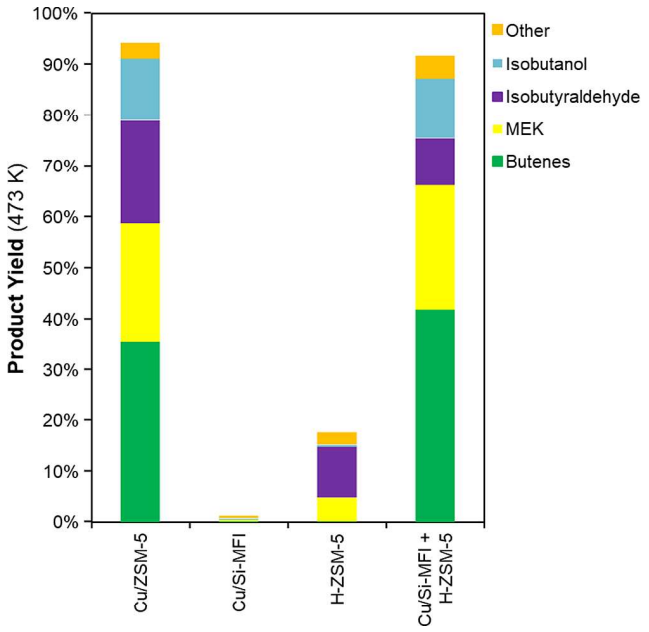

Figure 3. Product distributions from **3** conversion over Cu/ZSM-5, Cu/Si-MFI, and H-ZSM-5 and the physical mixture of Cu/Si-MFI and H-ZSM-5 taken at 3 h time-on-stream (5 kPa dioxolane in 96 kPa H_2, 473 K, 2.38 h^{-1} WHSV over Cu/ZSM-5, Cu/Si-MFI, and H-ZSM-5 or 1.18 h^{-1} over the physical mixture). Residual product distribution percentages reflect remaining dioxolane reactant at sub-100% conversion. Errors in product distributions are 12% under these conditions. The "Other" category combines C_5–C_9 alkenes with trace butane, ethylene, propene, and propane.

to a lack of ether protonation reactivity by Cu sites or other surface species, such as silanols, under these reaction conditions. The lack of acetoin or BDO in the product stream indicates that successive ether cleavage steps effectively separate the oxygen atoms between the two formed product molecules. Interestingly, isobutyraldehyde and MEK formed over H-ZSM-5 are observed in a ~2:1 molar ratio favoring isobutyraldehyde rather than the 1:1 ratio expected for cleanly separating the dioxolane at both ether groups. This phenomenon has been previously observed,[33] yet an in-depth mechanistic analysis is beyond the scope of this work. Here, the presence of Brønsted acid sites such as those present on H-ZSM-5 is critical for catalyzing the initial ether cleavage steps of the dioxolane conversion reaction pathway.

When **3** is converted over Cu/ZSM-5 containing both Cu and Al sites, the product stream contains MEK and isobutyraldehyde along with butanol and butene isomers as substantial products (Figure 3). Since MEK and isobutyraldehyde result from ether cleavage reactions over Al Brønsted acid sites, butanol isomers (e.g., isobutanol, 2-butanol) reflect the hydrogenation of either isobutyraldehyde or MEK, respectively. Cu sites are well-known for their aldehyde hydrogenation reactivity under similar reaction conditions with decreased alkene hydrogenation reactivity.[48−50] Butene isomers can then be formed from the dehydration of butanol, where Brønsted acid sites are well-known for catalyzing dehydration reactions. This proposed mechanism for the formation of alkenes from dioxolanes is shown in Scheme 2 using **3** as a representative dioxolane. Scheme 2 can be readily extended to additional dioxolanes studied here.

Notably, dioxolane conversion is significantly higher over Cu/ZSM-5 than over Cu-free H-ZSM-5 with higher MEK and isobutyraldehyde partial pressures. Since Cu sites alone do not catalyze the initial ether cleavage steps, higher dioxolane conversion over Cu/ZSM-5 can reflect one of two phenomena: the formation of Cu-exchanged Al Brønsted acid sites that catalyze dioxolane cleavage with greater reactivity than Brønsted acid sites alone or the removal of intermediates such as MEK or isobutyraldehyde, which potentially competitively adsorb onto Brønsted acid sites and decrease the number of ether cleavage active sites. The first proposed explanation was investigated using a physical mixture of Cu/Si-MFI and H-ZSM-5 where the Cu and Al active sites are separated in space. As seen in Figure 3, product distributions measured over the physical mixture and over Cu/ZSM-5 are quite similar, and the physical mixture possesses higher dioxolane conversion reactivity than H-ZSM-5 alone with an overall dioxolane conversion closer to that observed over Cu/ZSM-5 (see Figure S9 for a direct comparison of the transient behavior of Cu/ZSM-5 and the physical mixture). Further, the physical mixture largely resists the rapid deactivation observed over H-ZSM-5. These physical mixture results indicate that the Cu and Al sites do not require close proximity to catalyze their respective reactions within the dioxolane-to-alkenes pathway and circumstantially suggest the necessity of hydrogenation sites to convert intermediate species that competitively adsorb onto Al Brønsted acid sites, maintaining higher ether cleavage rates as a function of time.

Overall, the product distributions and yields presented in Figures 2 and 3 indicate the catalytic relevance of both Al and Cu sites for facilitating the cascading dioxolane-to-alkene reaction network proposed in Scheme 2. Dioxolane conversion appears to undergo multiple ether cleavage steps to cleave the dioxolane at the oxygens to form MEK and the parent aldehyde followed by carbonyl hydrogenation to form alcohols and dehydration to form alkenes. This proposed mechanism is similar to those proposed over other catalysts for dioxolane conversion[33,51] and is in alignment with previous mechanisms for dioxolane formation.[52] Cu/ZSM-5 contains all relevant

Scheme 2. Proposed Reaction Pathway for Dioxolane Conversion into Alkenes Using 3 As an Example[a]

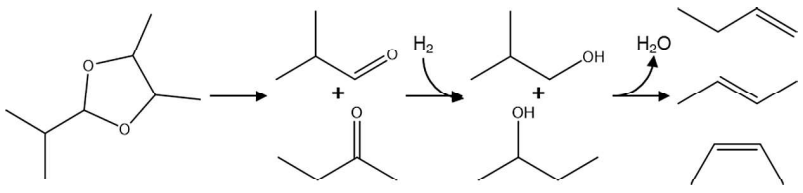

[a]**3** is derived from isobutyraldehyde and BDO. Reaction steps include ether cleavage, hydrogenation, and dehydration to yield a butene-rich alkene product mixture.

https://doi.org/10.1021/acssuschemeng.4c01155
ACS Sustainable Chem. Eng. XXXX, XXX, XXX−XXX

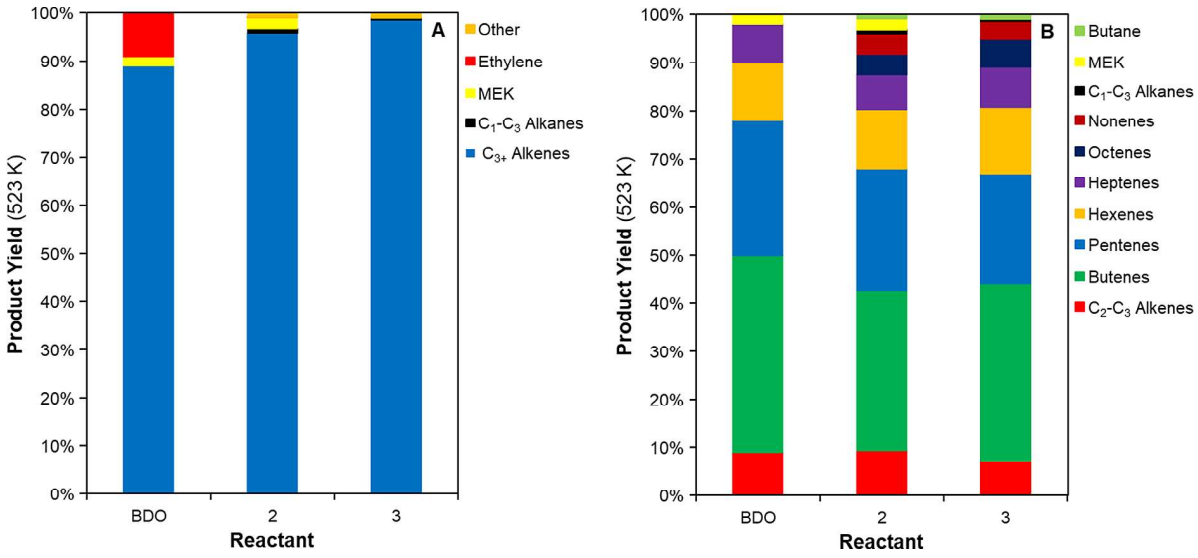

Figure 4. Grouped (A) and detailed (B) product distributions derived from the conversion of BDO, **2**, and **3** over Cu/ZSM-5 at 523 K (0.375 cm^3 s^{-1} H_2, 0.8−1.0 h^{-1} WHSV, ~0.005 mol (g catalyst)$^{-1}$ h^{-1}). Errors in product distributions are 12% under these conditions. The "Other" category in (A) combines trace butanol and butane.

active sites for facilitating the entire reaction pathway just as it has for direct BDO conversion.[9]

Since Cu/ZSM-5 has been demonstrated as an effective catalyst for the conversion of both BDO and dioxolanes to alkenes, a direct comparison can be made between the two reactants, where the latter reactant is derived from BDO and could represent a better process for BDO conversion into C_{3+} alkenes. Figure 4 shows measured product distributions derived from the thermocatalytic conversion of BDO and dioxolanes **2** and **3** derived from BDO and either butyraldehyde or isobutyraldehyde respectively over Cu/ZSM-5 using consistent operating conditions (523 K, 0.8−1.0 h^{-1} WHSV). Reactant flow rates were controlled to maintain a constant molar flow rate over the Cu/ZSM-5 catalyst and therefore a constant reactor residence time. The simplest BDO-to-alkenes reaction network combines two dehydration steps and a single hydrogenation step to form butene[9] while the dioxolane-to-alkenes reaction network proposed in Scheme 2 combines two ether cleavage steps, two hydrogenation steps, and two dehydration steps to yield two moles of butene with one molar equivalent ultimately derived from BDO. Thus, at a fixed reactant molar flow rate for BDO and the two dioxolanes, dioxolane conversion requires additional steps, can generate more potential intermediates, and handles twice the total carbon amount over the same Cu/ZSM-5 catalyst loading and corresponding active site concentrations. A lower total alkene yield would then be understandable, given the increased complexity of dioxolane conversion relative to BDO; however, alkene yields are higher for dioxolane conversion than for pure BDO (96% vs 89% yield, 100% conversion, 523 K).

Figure 4A combines all C_{3+} alkenes together since the formation of these compounds is the primary goal for eventual fuel generation, and Figure 4B depicts the more detailed alkene distributions. BDO, **2**, and **3** are all completely converted at this temperature and space velocity, and minimal differences are observed between the product distributions derived from the three reactants. Indeed, product distributions derived from both **2** and **3** show increased selectivity toward C_{3+} alkenes (95+%) over direct BDO conversion (89%). This indicates that dioxolane conversion pathways are not only equivalent to BDO conversion but also can outcompete direct BDO conversion for the formation of desired alkene products. The presence of longer carbon chain alkenes in these product distributions indicates various metathesis or oligomerization and cracking reactions previously observed with BDO-to-alkenes formation,[9] yet bulk C_{3+} alkene distributions remain butene-rich (35−41%, Figure 4B) as expected from the C_4 chain lengths of BDO and BDO- and aldehyde-derivatives from **2** and **3** conversions. Small amounts (<3%) of MEK and the parent aldehyde indicate incomplete hydrogenation over the Cu/ZSM-5 catalyst which would further increase the butene yield if these species were hydrogenated and dehydrated, allowing for additional optimization of reaction conditions or catalytic active sites on Cu/ZSM-5. However, this Cu/ZSM-5 catalyst can catalyze the conversion of both BDO and dioxolane reactants, notably converting both the BDO and aldehyde components of the dioxolane into butene isomers.

Upon identification of Cu/ZSM-5 as a useful catalyst for dioxolane conversion, a larger range of dioxolanes were investigated for alkene formation at various reaction temperatures. Figure 5 shows high conversion product distributions (473−523 K, ~5 kPa dioxolane in balance H_2) derived from the conversion of the range of dioxolane compounds shown in Table 1. In general, each product distribution primarily consists of C_{3+} alkenes including C_{9+} alkenes coupled together under the nonene label, C_1−C_3 alkanes, MEK and butanol isomers as BDO derivatives, and aldehydes and alcohols with carbon chains matching the parent aldehyde used for dioxolane formation (labeled "Other Aldehyde" and "Other Alcohol," respectively; see Figures S10 and S11 for more detailed product distributions and selectivity figures). As an example, the other aldehydes and alcohols from the conversion of **7** are 2-ethylhexanal and 2-ethylhexanol, respectively. This labeling scheme allows for a ready comparison of aldehyde and alcohol yields derived from the aldehyde-derived dioxolane component. Trace side products include diethyl ether, butane, and

https://doi.org/10.1021/acssuschemeng.4c01155
ACS Sustainable Chem. Eng. XXXX, XXX, XXX−XXX

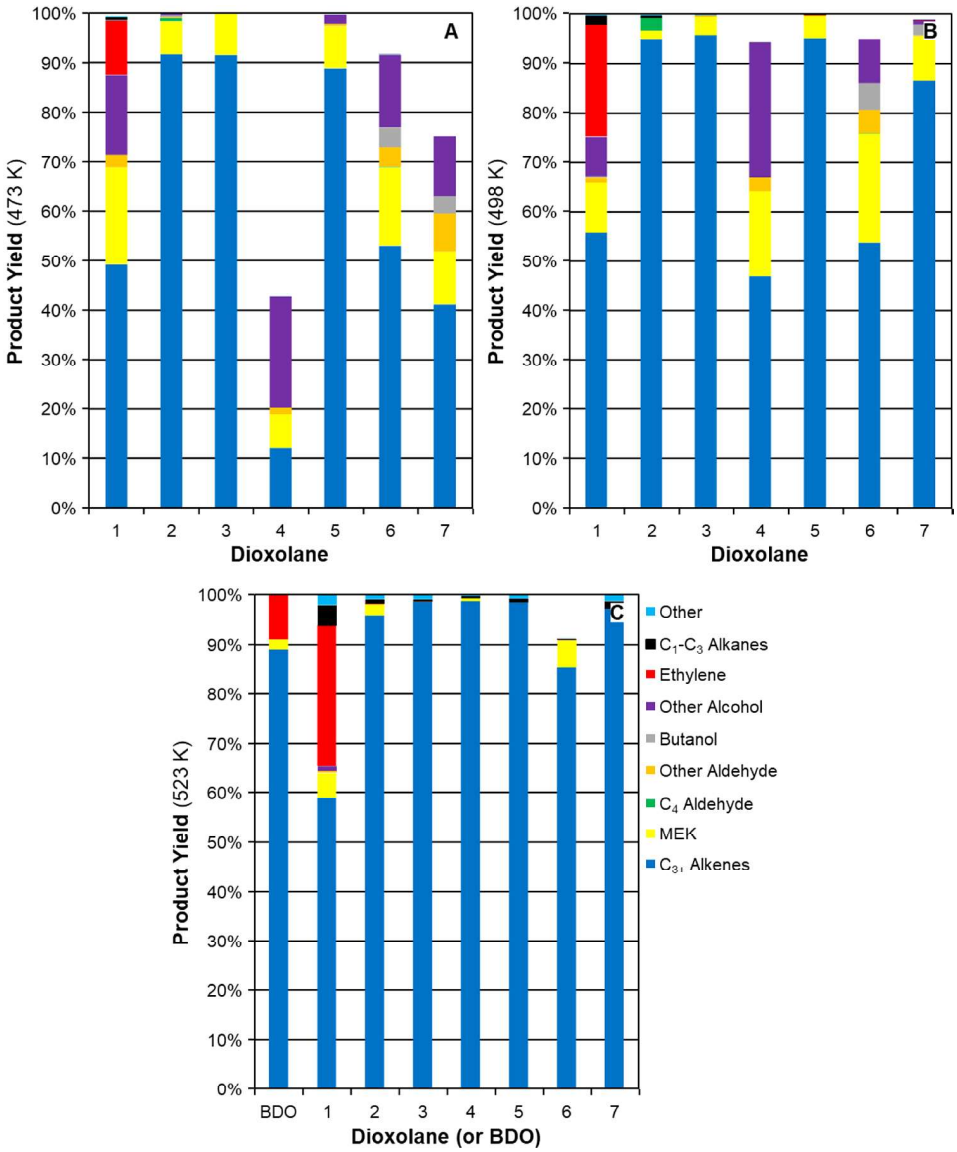

Figure 5. Dioxolane conversion product distributions obtained over Cu/ZSM-5 at (A) 473 K, (B) 498 K, and (C) 523 K (0.375 $cm^3 s^{-1}$ H_2, 0.8–1.1 h^{-1} WHSV, ~0.0055 mol (g catalyst)$^{-1}$ h^{-1}) as a function of dioxolane side chain. WHSV was varied to maintain a constant reactant molar flow rate. Residual product distribution percentages reflect remaining dioxolane reactant at sub-100% conversion. Errors in product distributions are 12% under these conditions. The "Other" category combines butane and diethyl ether.

acetone which are labeled as "Other." Furthermore, despite each dioxolane feed containing a mixture of all three stereoisomers, limited reactivity differences are observed between the various isomers under these conditions.

Interestingly, dioxolanes derived from branched aldehydes (e.g., isobutyraldehyde, 2-ethylbutanal, and 2-ethylhexanal) have higher conversions than dioxolanes derived from linear aldehydes. Despite conversion differences, observed product distributions collected at 473 K primarily show two product groupings: one comprised of C_4 compounds, and another comprised compounds matching the carbon chain length of the parent aldehyde utilized for dioxolane formation (Figure 5A). The molar ratio between C_4 compounds and the associated carbon length of the parent aldehyde are given in Table 3 at 273 and 498 K. For the conversion of **1**, the dioxolane derived from the reaction of BDO and acetaldehyde, product distributions depict butene isomers and MEK as well as ethanol ("Other Alcohol"), ethylene, and acetaldehyde

Table 3. Molar Ratios of Dioxolane Conversion Products over Cu/ZSM-5 as a Function of the Temperature[a]

dioxolane number	aldehyde carbon chain length	C_4 selectivity (%)[b]	$C_{aldehyde}$ selectivity (%)[b]	C_4/$C_{aldehyde}$ molar ratio[b]	C_4/$C_{aldehyde}$ molar ratio[c]
1	2	58.8	27.8	1.0	0.9
2	4	89.2			
3	4	91.6			
4	6	22.3	71.7	0.5	0.7
5	6	35.3	59.0	0.9	1.4
6	8	34.0	55.5	1.2	1.4
7	8	27.6	55.5	1.0	1.1

[a]C_4 and $C_{aldehyde}$ selectivity values couple together all products of those carbon chain lengths. [b]Derived from product distributions measured at 473 K. [c]Derived from product distributions measured at 498 K.

https://doi.org/10.1021/acssuschemeng.4c01155
ACS Sustainable Chem. Eng. XXXX, XXX, XXX−XXX

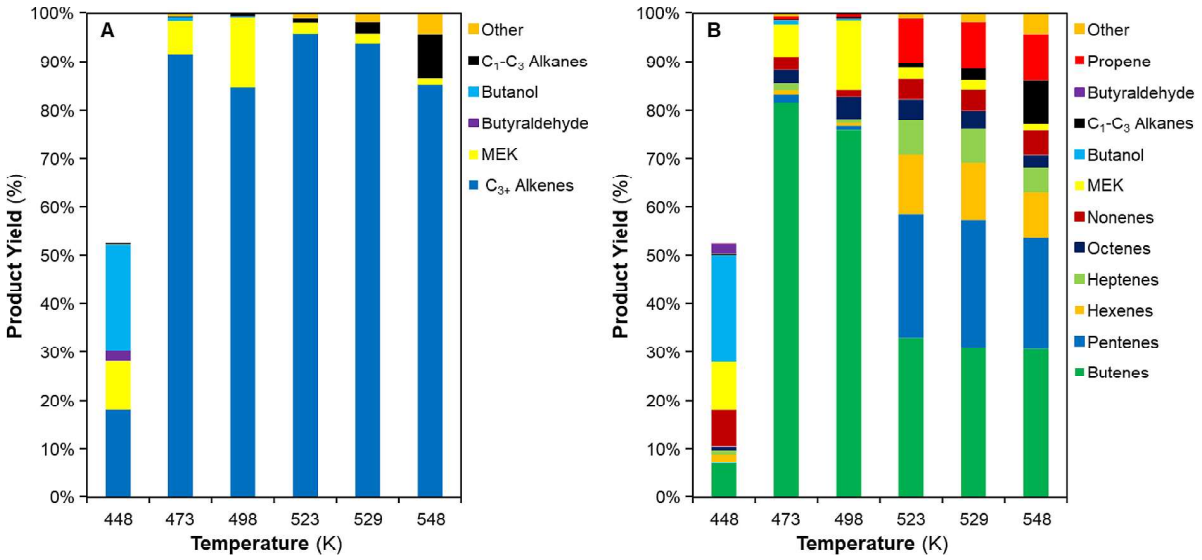

Figure 6. (A) Bulk and (B) detailed product distributions measured from the conversion of **2** over Cu/ZSM-5 (0.375 cm^3 s^{-1} H_2, 0.8 h^{-1} WHSV, and 0.0055 mol (g catalyst)$^{-1}$ h^{-1}) as a function of temperature. Residual product distribution percentages reflect remaining dioxolane reactant at sub-100% conversion. Errors in product distributions are 12% under these conditions. The "Other" category combines butane, ethylene, and trace C_8 oxygenates.

("Other Aldehyde) as the two primary product groupings. **2** and **3** derived from BDO and butyraldehyde or isobutyraldehyde, respectively, primarily yield product distributions that highly favor butene isomers and MEK while **6** and **7** derived from BDO and octanal or 2-ethylhexanal respectively yield significant amounts of both C_4 (e.g., butene isomers, MEK) and C_8 compounds (e.g., octene, octanal, and octanol isomers). The presence of aldehydes and alcohols of various carbon chain lengths as well as MEK at 473 K reflects insufficient hydrogenation and dehydration rates to form the associated alkenes (Scheme 2). Increasing the temperature to 498 K increases the overall conversions above 90% for all studied dioxolanes (Fig. 5B). Relative aldehyde or alcohol yields decrease in favor of increased alkene yields, indicating increased hydrogenation and dehydration reactivity. The carbon chain lengths of the alkene mixtures maintain increased selectivity towards butene and alkenes matching the carbon chain length of the parent aldehyde, indicating minimal metathesis and various oligomerization and cracking reactions of formed alkenes.

The reaction temperature could be further increased to hypothetically drive hydrogenation and dehydration rates toward completion and maximize C_{3+} alkene formation. At 523 K (Figure 5C), the temperature previously investigated for pure BDO conversion over Cu/ZSM-5,[9] complete dioxolane conversion is observed for nearly all dioxolanes with combined C_{3+} alkene yields that are often above 85%. While alkene compositions span a range of carbon chain lengths from ethene to nonenes and longer, product distributions look similar within error regardless of selected dioxolane reactant (Figures S10 and S11). This indicates a redistribution of carbon chain lengths between the aldehyde and BDO components to a seemingly "equilibrated" mixture of alkenes regardless of each dioxolane's initial side chain length or configuration, reflecting a series of metathesis and oligomerization or cracking reactions that reconfigure carbon chain lengths. Additionally, alkanes ranging from methane to butane were observed at low but detectable partial pressures (<2%), indicating the onset of undesirable alkene hydrogenation. These side reactions become significantly more pronounced at elevated reaction temperatures (523 vs 473−498 K), trading higher conversions for selectivity toward less desired final products. While alkane generation is highly undesirable due to their limited chemical reactivity relative to alkenes, the mixed alkene product distributions derived from metathesis and/or oligomerization and cracking reactions are still suitable for bulk oligomerization for aviation fuel generation. Traditional oligomerization reactors are accustomed to processing mixed alkene distributions, yet product distributions targeting specific alkene lengths could be surmised using the dioxolane conversion pathway.

While lower reaction temperatures yield more controllable alkene compositions, overall dioxolane conversion and hydrogenation and dehydration rates increase with increasing temperature. This can be more clearly observed in Figure 6 which depicts product yields as a function of temperature derived from the conversion of **2** over Cu/ZSM-5 (see Figures S12−S14 for product distributions and selectivities derived from **1**, **3**, and **7** as a function of temperature). Below 473 K, the conversion of **2** drops to ∼50% due to substantially decreased ether cleavage rates, and the observed product distribution yields primarily C_4 compounds, including butene isomers, MEK, and butanol isomers. Complete conversion is observed at and above 473 K with 85+% selectivity toward butene isomers at 473 and 498 K. Residual MEK reflects incomplete hydrogenation, yet minimal shorter or longer carbon chain alkenes indicate negligible rates of metathesis, isomerization, oligomerization, and cracking. As the temperature is increased further, C_{3+} alkene selectivities remain high, yet short-chain alkenes (e.g., ethylene and propene) and their hydrogenated alkane equivalents become increasingly present, generating undesirable products while consuming additional hydrogen gas. Additionally, C_{3+} alkene distributions shift from primarily butene isomers to a wide range of alkenes. Taken together, this suggests an optimal temperature range of 498−523 K for maximizing dioxolane conversion without minimizing undesirable side reactions that form shorter carbon chain

https://doi.org/10.1021/acssuschemeng.4c01155
ACS Sustainable Chem. Eng. XXXX, XXX, XXX−XXX

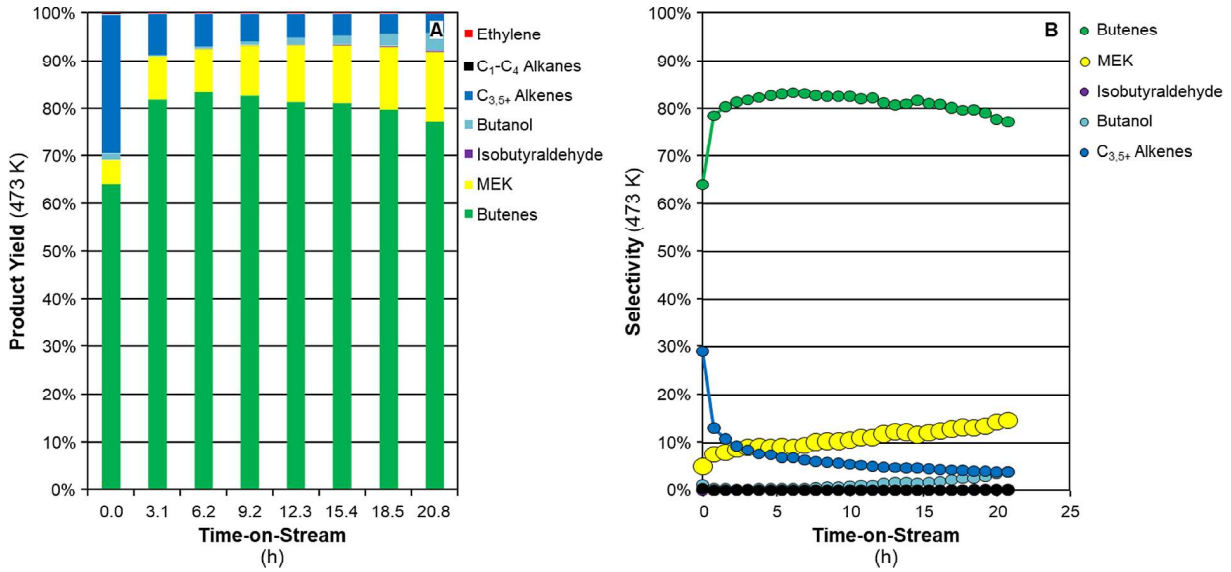

Figure 7. (A) Transient product distributions and (B) product selectivity from the conversion of **3** over Cu/ZSM-5 (~5% dioxolane in H_2, 473 K, 0.8 h^{-1} WHSV). Errors are 12% under these conditions.

alkenes or fully hydrogenated alkanes. This optimal temperature range holds for dioxolanes derived from other aldehydes (Figures S12–S14).

Another key aspect for assessing the viability of the proposed BDO-to-dioxolane-to-alkenes process is the stability of the Cu/ZSM-5 catalyst. While the high conversion product distributions shown in Figures 5 and 6 reflect the full dioxolane conversion reaction network at discrete times-on-stream, Figures 7 and 8 probe catalyst stability at both high and low steady-state conversions, respectively. Figure 7 depicts the high conversion catalytic stability of Cu/ZSM-5 at 473 K using **3** as a representative dioxolane reactant. These high conversion conditions were used to investigate changes throughout the cascading dioxolane-to-alkene reaction network in the presence of the full range of intermediates and products that would be present under industrially relevant conditions. Transient product distribution differences can be evaluated to qualitatively investigate changes in the multiple reaction steps and associated active sites. Product distributions collected at initial times indicate high selectivity toward butene isomers (~65%), some alkenes with both longer and shorter carbon chain lengths than butene, and small amounts of MEK. Negligible alkane formation was detected.

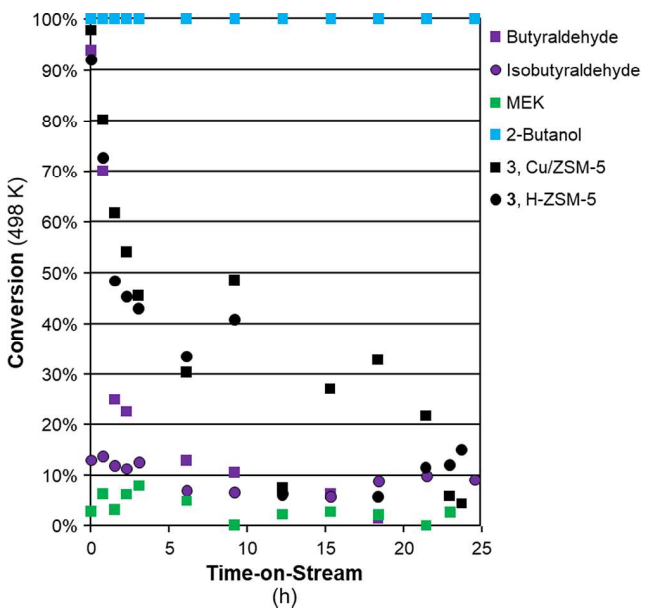

Figure 8. Transient conversion of butyraldehyde, isobutyraldehyde, MEK, 2-butanol, and **3** over Cu/ZSM-5 (498 K, ~5 kPa reactant in H_2, 11.9 h^{-1} WHSV). The conversion of **3** over H-ZSM-5 (2.4 h^{-1} WHSV) is included for comparison. Detailed transient product distributions from each reactant are shown in Figure S15.

After initial catalyst degreening (~2–3 h), butene selectivity is maximized at ~83% alongside decreased selectivity toward other alkene products, indicating the mitigation of metathesis or related reaction steps due to the deactivation of those active sites. This deactivation could be caused by either coke formation or competitive adsorption of other intermediates or products. At longer TOS, butene selectivity slowly begins to decrease, while MEK selectivity increases stoichiometrically, indicating decreased hydrogenation or dehydration reactivity required for MEK conversion into butene. Similarly, butanol selectivity begins to increase at longer TOS primarily in the form of isobutyraldehyde alongside low amounts of isobutyraldehyde. This indicates an incremental decrease in the dehydration reactivity of isobutanol to isobutene, which could reflect the deactivation of the Al Brønsted acid sites responsible for dehydration. The isobutanol/isobutyraldehyde components are primarily derived from the parent isobutyraldehyde utilized for initial **3** formation and favor the reduced product of isobutanol while MEK and trace 2-butanol are derived from BDO with MEK as the more energetically favorable product. Therefore, the deactivation phenomena associated with downstream steps of the cascading dioxolane-to-alkene reaction network cannot be easily attributed to one specific set of active sites or reaction intermediates.

To further probe potential catalyst deactivation mechanisms, MEK, 2-butanol, and butyraldehyde were independently converted over Cu/ZSM-5 (498 K) with overall conversion as a function of time plotted in Figure 8 (see Supplementary Figure S15 for transient product distributions derived from

https://doi.org/10.1021/acssuschemeng.4c01155
ACS Sustainable Chem. Eng. XXXX, XXX, XXX−XXX

each reactant). Figure 8 also depicts the deactivation profiles for the conversion of **3** over Cu/ZSM-5 and H-ZSM-5 for a direct comparison. Catalyst masses were decreased from previous high conversion measurements to observe deactivation phenomena more directly, and a consistent molar flow of the liquid reactants was maintained across all experiments. Reactions were performed at 498 K as this temperature reflects the maximum butene selectivity (Figure 5) without the alkene carbon chain scattering observed at higher reaction temperatures. Products formed from each of these reactants reflect the reaction network proposed in Scheme 2 (i.e., alkenes and 1-butanol from butyraldehyde, alkenes alone from 2-butanol, etc.).

The conversion of butyraldehyde is nearly 100% at early TOS yet deactivates quickly. Butyraldehyde conversion primarily forms butene isomers at initial times, yet alkene formation quickly deactivates in favor of near-100% selectivity to 1-butanol, indicating decreased dehydration rates with TOS likely from the loss of dehydration sites. Steady-state butyraldehyde conversion levels out around 10% under these conditions. In contrast, isobutyraldehyde conversion remains low yet consistent (~10%) across the 25 h reaction and does not see significant deactivation, matching the steady state butyraldehyde conversion. Transient MEK conversion mirrors isobutyraldehyde, remaining low yet fairly steady; lower MEK hydrogenation rates than isobutyraldehyde or butyraldehyde explain the presence of residual MEK in dioxolane conversion product distributions (Figures 5 and 6). At these temperatures, catalyst loadings could not be reasonably lowered enough to drop 2-butanol conversions below 100%, yet the formed products shift from an alkene mixture toward ~95% butene selectivity (Figure S15D). This high dehydration reactivity of 2-butanol and the lack of isobutanol observed in the conversion of isobutyraldehyde contrasts the 1-butanol dehydration behavior seen during butyraldehyde conversion. MEK and isobutyraldehyde are either fully converted to butene or other alkenes or remain unreacted while butyraldehyde rapidly hydrogenates. This behavior is generalizable for linear aldehydes studied in Figure 5B: product distributions collected at 498 K from the conversion of **4** and **6** have higher alcohol yields than those of dioxolanes formed from branched aldehydes.

The transient conversions of key intermediate species can be directly compared with the conversion of **3** over Cu/ZSM-5. Deactivation is slower for the total dioxolane conversion, and the observed product distributions favor MEK and isobutyraldehyde over alkenes or butanol. Here, catalyst deactivation reflects decreasing ether cleavage rates with deactivation rates that are ~5× lower over Cu/ZSM-5 than over H-ZSM-5 (Figure 8). Since the physical mixture experiments shown in Figure 2 indicate minimal Cu exchange onto Al Brønsted acid sites, this increased deactivation over H-ZSM-5 is likely caused by competitive adsorption of intermediate species onto Al Brønsted acid sites. Notably, competitive adsorption onto each set of active sites is dependent on the partial pressures of each reactant, intermediate, and product such that the deactivation observed from feeding key intermediates does not directly map onto high conversion measurements or measurements sampling the full dioxolane conversion reaction network. These competitively adsorbing species are reacted off via hydrogenation when Cu is present, leading to 5x greater catalyst stability over Cu/ZSM-5 relative to H-ZSM-5. Therefore, controlling hydrogenation rates of MEK, isobutyraldehyde, and other aldehydes will be critical for the commercial application of the dioxolane-mediated BDO-to-alkenes process investigated here.

To further investigate the role of competitive adsorption on observed catalyst deactivation, a stripping experiment was performed over H-ZSM-5 after the catalyst was allowed to deactivate. Stripping experiments investigate the removal of reversibly adsorbed compounds under reaction conditions but without introducing a new reactant. Figure 9 shows transient

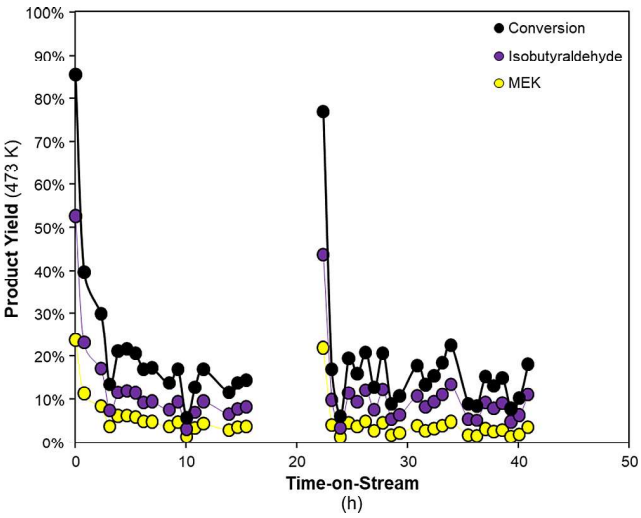

Figure 9. Transient conversion of **3** over H-ZSM-5 (473 K, ~5 kPa reactant in H_2, 2.4 h^{-1} WHSV). The gap from ~16 to 22 h reflects the stripping period where no additional liquid reactant was introduced to the reactor and formed products and intermediates are desorbed.

dioxolane **3** conversion and key product yields at 473 K over H-ZSM-5 where the catalyst was first allowed to deactivate for ~16 h time-on-stream. The dioxolane reactant flow was then shut off for ~6 h, while a constant H_2 flow was maintained at the reaction temperature, allowing for the reaction of adsorbed dioxolane species and bulk desorption of bound species. GC-FID spectra show the rapid disappearance of dioxolane reactant peaks followed by a slower decrease and eventual disappearance of dioxolane ether cleavage products including MEK and isobutanal. Once the product peaks had disappeared, the surface and associated catalytic active sites were assumed to be clean of adsorbed intermediates, and the syringe pump was restarted for additional data collection. Notably, both the overall dioxolane conversion and respective isobutyraldehyde and MEK yields are nearly fully recovered (within 10% of the initial reactivities) after the desorption period. Therefore, the observed deactivation is largely reversible without oxidation or another regenerative procedure, indicating that Brønsted acid site deactivation is not caused by coke or titration and instead is caused by the competitive adsorption of intermediates. Comparing this deactivation profile with the conversion of **3** over Cu/ZSM-5 (Figure 2) indicates mitigated deactivation when Cu species are present. Within this reaction network, this mitigation likely reflects the hydrogenation of MEK and the aldehyde over Cu sites and thus decreased chemical potentials and associated coverages of these oxygenates onto the Brønsted acid sites. Further catalyst deactivation studies will be investigated in the future to improve the catalyst stability for commercial applications.

https://doi.org/10.1021/acssuschemeng.4c01155
ACS Sustainable Chem. Eng. XXXX, XXX, XXX−XXX

CONCLUSIONS

We have investigated the use of dioxolane synthons for a BDO-to-alkenes reaction pathway pointed toward the generation of aviation fuels. Dioxolanes can recover BDO from aqueous media via reactive separation that avoids critical barriers for BDO separation and purification and can then be converted into C_{3+} alkene mixtures over Cu/ZSM-5 at greater yields (>95%, 523 K) than those measured from direct BDO conversion. These BDO-derived dioxolanes can be synthesized with >90% yield utilizing a wide range of aldehydes, increasing process versatility with renewable aldehyde availability and affordability. Dioxolane conversion over Cu/ZSM-5 proceeds via two ether cleavage steps over Al Brønsted acid sites to form MEK and the parent aldehyde, hydrogenation of MEK and the aldehyde into alcohols over Cu sites, and dehydration of the alcohols into alkene mixtures over Al Brønsted acid sites. At reaction temperatures below 523 K, the carbon chain lengths of both BDO and the parent aldehyde can be maintained in the product distributions as either alkenes or aldehydes and alcohols, allowing for controlling the final alkene composition without necessarily sacrificing overall dioxolane conversion. Higher temperatures allow for metathesis, oligomerization and cracking, and alkene hydrogenation steps over Cu/ZSM-5 that can shuffle alkene chain lengths and form shorter alkenes and alkanes, limiting the C_{3+} alkene yields useful for downstream oligomerization and hydrotreating to generate sustainable aviation fuel. Catalyst deactivation occurs for each step of the cascading reaction network, yet deactivation can be minimized at 498 K by processing the entire dioxolane-to-alkene reaction network simultaneously, indicating complex competitive adsorption effects from various intermediates formed along the way.

Overall, the use of dioxolanes as BDO synthons avoids critical barriers for BDO utilization as a renewable fuel feedstock and can increase overall C_{3+} alkene yields using a simple Cu/ZSM-5 synthetic procedure and commercially available catalyst supports. However, this dioxolane formation and conversion process typically consumes the aldehyde under the reaction conditions investigated in this work and therefore would require a low-cost aldehyde to be consistently fed into the dioxolane formation reactor. This aldehyde would likely be derived from petroleum until either a sufficiently inexpensive and renewably sourced aldehyde was generated at a commercial scale or the dioxolane conversion reactor could be tailored to recapture aldehydes after dioxolane cleavage steps. Future work will investigate process improvements that can facilitate aldehyde recovery and recycling to minimize aldehyde losses and improve technoeconomic and life-cycle assessments.

EXPERIMENTAL METHODS

Dioxolane Syntheses and Characterization. Dioxolane compounds were synthesized from BDO and an aldehyde by adapting a previously published method.[31] Typically, 18 g of BDO was added to 1.7 g of Amberlyst-15 (Sigma-Aldrich, 216380, 5.1 mmol g^{-1} H^+ density[38]) in a Teflon-lined stainless-steel autoclave (45 cm^3, Parr Instruments) followed by the desired aldehyde. The mass of the aldehyde was adjusted to maintain a 1.5:1 aldehyde:BDO molar ratio. The autoclave was then sealed and heated to 313 K for 6 h while rotating (30 rpm) in an isothermal oven (VWR 1350FM oven) prior to being cooled to room temperature. The resulting mixture was left for 0.25 h to settle into distinct organic and aqueous phases above solid Amberlyst-15. For dioxolanes synthesized using acetaldehyde, an apparent phase separation between the liquid solutions was not observed until after a small amount of water (5−10 mL, 18.2 MΩ) was added. The organic layer was decanted and used without additional purification. BDO recovery exceeds 95% under these conditions which is consistent with previous reports.[31]

Dioxolane purity was assessed via NMR and gas chromatography−mass spectrometry (GC−MS). ^1H and ^{13}C NMR spectra were collected on a Bruker Avance AV400 MHz spectrometer at ambient temperature in $CDCl_3$. ^1H (400 MHz) and ^{13}C (101 MHz) spectra were referenced relative to tetramethylsilane, and chemical shifts were recorded in parts per million (ppm). GC−MS measurements were obtained on an Agilent 5975C GC−MS.

Catalyst Synthesis. Cu/ZSM-5 materials were synthesized via ammonia deposition using a previously reported procedure.[53,54] Commercial MFI (Zeolyst CBV28014, Si/Al = 140) was thermally treated in air (250 cm^3 min^{-1} (g solids)$^{-1}$, Airgas, Ultra Zero grade) to 823 K (5 K min^{-1}) for 6 h to remove any adsorbed species. The recovered solids provide support for Cu incorporation via liquid-phase ammonia deposition. In a typical deposition experiment, 0.76 g of $Cu(NO_3)_2{\cdot}3H_2O$ (Sigma-Aldrich, 99−104%) was added to 4 g of water (18.2 MΩ). Aqueous NH_4OH solution (Acros Organics, 25%) was added dropwise to the Cu-containing solution until a pH of 9.0−9.1 was achieved (Fisher Scientific, AE150). Water was then added to the solution to achieve 8 cm^3 of total liquid prior to the addition of 1 g of the calcined MFI and a stir bar. The mixture was then stirred for 4 h at room temperature, followed by heating to 353 K in an oil bath for 2 h while stirring prior to cooling back to room temperature. The resulting solids were washed with water (15 cm^3 (g catalyst)$^{-1}$), centrifuged, and decanted three times prior to drying overnight at 373 K. The solids were then thermally treated in air (1000 cm^3 min^{-1}) at 2 K min^{-1} to 373 K, held for 0.5 h, heated further at 5 K min^{-1} to 823 K, held for 4 h, and then cooled back to room temperature. The resulting solids comprise the Cu/ZSM-5 catalyst material utilized here.

Catalyst Characterization. Powder X-ray diffraction (XRD) patterns were measured by using a PANalytical X'Pert Pro MPD equipped with an X'Celerator solid-state detector. Measurements range from 4° to 80° (2θ) with a scan rate of 0.03° s^{-1} and a 0.017° step size. N_2 adsorption isotherms (77 K) were measured using a Quantachrome Autosorb iQ. ~ 0.03 g of pelletized and sieved sample (125−180 μm) was loaded into the instrument and degassed under vacuum (<0.002 Torr) first at 393 K (0.0833 K s^{-1}) for 1 h and then at 623 K (0.0833 K s^{-1}) for 6 h prior to adsorption experiments. Micropore volumes were quantified from a semilog derivative ($\delta(V_{ads}$ $g^{-1})/\delta(\log(P/P_0)$ vs $\log(P/P_0)$) analysis of N_2 adsorption isotherms. Bulk Cu and Al densities of zeolite samples were measured at Galbraith Laboratories, Inc., using inductively coupled plasma atomic emission spectroscopy (ICP-AES).

High-resolution (HR) scanning transmission electron microscopy (STEM) imaging was performed on an aberration-corrected JEOL JEM-ARM200F NEOARM TEM/STEM operated at 200 kV with a cold field emission gun (Cold-FEG), a next-generation Cs probe corrector (ASCOR) and energy dispersive X-ray spectroscopy (EDS) system with dual JEOL 100 mm^2 silicon-drift detectors (SDD) for chemical analysis. High-resolution analysis was performed with a nominal beam current of ~25 pA and an associated nominal resolution of 0.7 Å. For STEM analysis, the catalysts were drop-cast onto Carbon Coated 200 Mesh Gold Grids 3 mm grids (SPI Supplies part no. 3820GH-CF) from isopropanol suspensions.

N_2O temperature-programmed reduction (TPR) measurements were performed on an Altiamira AMI-300 instrument system equipped with an OmniStar GSD-301 (Pfeiffer Vacuum) online quadrupole mass spectrometer (MS) using an adaptation of a previously published method.[46,55] ~0.03 g of sample (125−180 μm) was loaded between quartz wool plugs in a U-tube reactor. Samples were thermally oxidized in 5% O_2 in Ar (50 cm^3 min^{-1}, Airgas) by heating to 823 K (5 K min^{-1}), holding for 1 h, and cooling to 323 K until the temperature was stabilized (~0.25 h). H_2 was introduced to the sample (4% H_2 in Ar, 50 cm^3 min^{-1}, Airgas) for 1 h prior to measuring the first H_2 TPR. While measuring H_2 consumption using online MS, the sample was heated to 673 K (5 K min^{-1}), held for 0.25

https://doi.org/10.1021/acssuschemeng.4c01155
ACS Sustainable Chem. Eng. XXXX, XXX, XXX−XXX

h, and then cooled to 363 K. Once cooled, the sample was flushed with 50 cm^3 min^{-1} of Ar (Airgas, Ultra High Purity) for 1 h prior to feeding 5% N_2O in He (50 cm^3 min^{-1}, Airgas) for 1.5 h. This has been reported to selectively oxidize surface Cu within CuO_x nanoparticles due to limited oxygen diffusion into metallic Cu nanoparticles.[46] The sample was then flushed with 50 cm min^{-1} Ar for 0.25 h to remove residual physisorbed N_2O prior to cooling to 323 K and holding for 0.5 h for the second H_2 TPR. 50 cm^3 min^{-1} concentration of 4% H_2 in Ar was introduced over the sample while measuring H_2 consumption. The sample was heated to 673 K (5 K min^{-1}), held for 0.25 h, and cooled back to room temperature. Transient MS was integrated for both H_2 TPR measurements to compare bulk H_2 consumption quantities from Cu reduction using the following previously published empirical relationship.[56]

$$d_{VS} = d_{Cu}{}^{*}\frac{3.32}{\left(2^{*}\frac{Cu_{surface}}{Cu_{total}}\right)^{1.23}} \quad (1)$$

Here, d_{VS} is the volume-surface mean diameter of the Cu nanoparticles, d_{Cu} is the atomic diameter of Cu, Cu_{total} is the total number of reducible Cu atoms measured by the first H_2 TPR, and $Cu_{surface}$ is the amount of surface Cu atoms measured by the second H_2 TPR.

NH_3 temperature-programmed desorption (NH_3 TPD) measurements were performed on an Altiamira AMI-300 instrument system equipped with an OmniStar GSD-301 (Pfeiffer Vacuum) online quadrupole mass spectrometer (MS) following a previously reported procedure for measuring Brønsted acid site densities on Al-containing MFI catalysts.[41] ~0.05 g of sample (125−180 μm) was loaded similarly to the N_2O TPR measurements. Samples were held in 10 cm^3 min^{-1} of H_2 (Airgas, Ultra High Purity) in 50 cm^3 min^{-1} Ar for 0.25 h, heated to 573 K (5 K min^{-1}), held for 1 h, cooled to 383 K, and flushed with 50 cm^3 min^{-1} Ar for 0.5 h prior to NH_3 adsorption. These conditions are analogous to the catalyst pretreatment conditions prior to dioxolane conversion measurements. After stabilization, 2% NH_3 in balance Ar (50 cm^3 min^{-1}, Airgas) was flowed over the sample for 1 h prior to switching to Ar (50 cm^3 min^{-1}) for 1.25 h at 433 K. The sample was then heated to 873 at 10 K min^{-1}, held for 0.5 h, and finally cooled to room temperature. NH_3 quantities were analyzed throughout the experiment via MS (m/z = 17), and m/z contributions from water were accounted for. A calibration was performed after each experiment for the NH_3 concentrations.

Dioxolane Conversion Measurements. Dioxolane conversion measurements were measured using a vertically aligned tubular quartz reactor (0.5 in. OD) under ambient pressure. Prior to the performance of dioxolane conversion experiments, each catalyst was pelletized, crushed, and sieved (125−180 μm). Typically, 0.15 g of catalyst was diluted in 0.6 g of silica carbide (SiC, Alfa Aesar, 120 grit) placed between two quartz wool beds (Chemglass, 8−15 μm) within the tubular reactor with a K-type thermocouple (Omega) positioned within the catalyst bed to monitor the catalyst bed temperature. Catalyst beds were pretreated to 573 K (5 K min^{-1}) in a reducing environment (10 cm^3 min^{-1} H_2 in 50 cm^3 min^{-1} Ar) and held for 1.5 h prior to cooling to the desired reaction temperature. Gas transfer lines were then set to bypass the catalyst bed and switched to 22.5 cm^3 min^{-1} H_2. Liquid dioxolanes were introduced via a syringe pump (KD Scientific Legato 180) into the preheated gas stream and vaporized. Liquid dioxolane flow rates were adjusted to maintain a constant molar flow rate and associated residence time within the reactor (67:1 H_2:dioxolane molar ratio). A consistent reactant flow was obtained via subsequent GC injections prior to switching the gas streamflow pattern over the catalyst bed. Dioxolane conversion background reactions using quartz wool, SiC, or Si-MFI show no discernible dioxolane conversion within the studied temperature range. Product distributions were measured using a gas chromatograph (Agilent 7820A) equipped with a flame ionization detector (GC-FID). Product mixtures were separated using an HP-PLOT-Q column (30 m, 0.32 mm diameter, 20 μm film) using known standards for product identification. Carbon balances were measured using 1-octane as an inert internal standard and are consistently above 95%.

Reactant conversions were determined based on peak area differences between stability measurements and product distributions. Conversion, product selectivity, and yield of species i were quantified via eqs 1−3:

$$\chi = \left(1 - \frac{\dot{n}_{reactant,out}}{\dot{n}_{reactant,in}}\right) \times 100 \quad (2)$$

$$S_i = \frac{n_{C,i}}{n_{C,prod}} \times 100 \quad (3)$$

$$Y_i = \frac{\dot{n}_{C,i}}{\dot{n}_{reactant,in}} \times 100 \quad (4)$$

Here, χ is conversion, $\dot{n}_{reactant,in}$ and $\dot{n}_{reactant,out}$ are the inlet and outlet reactant molar flow rates, S_i is the selectivity toward species i, $n_{C,i}$ is the moles of carbon in product i, and $n_{C,prod}$ is the combined moles of carbon in all detectable products. Y_i is the yield toward species i, and $\dot{n}_{C,i}$ is the product molar flow rates.

■ ASSOCIATED CONTENT

Supporting Information

The Supporting Information is available free of charge at https://pubs.acs.org/doi/10.1021/acssuschemeng.4c01155.

Dioxolane mass and NMR spectra, XRD patterns, N_2 adsorption isotherms, NH_3 TPD traces, additional HAADF-STEM images, H_2 TPR traces, detailed product distribution and selectivity figures, and additional transient conversion figures (PDF)

■ AUTHOR INFORMATION

Corresponding Authors

Michael J. Cordon − *Manufacturing Science Division, Oak Ridge National Laboratory, Oak Ridge, Tennessee 37830, United States*; orcid.org/0000-0002-5675-8027; Email: cordonmj@ornl.gov

Andrew D. Sutton − *Manufacturing Science Division, Oak Ridge National Laboratory, Oak Ridge, Tennessee 37830, United States*; orcid.org/0000-0001-7984-1715; Email: suttonad@ornl.gov

Authors

Meijun Li − *Manufacturing Science Division, Oak Ridge National Laboratory, Oak Ridge, Tennessee 37830, United States*

Xiaokun Yang − *Chemistry Division, Los Alamos National Laboratory, Los Alamos, New Mexico 87545, United States*

Peter G. N. Neate − *Chemistry Division, Los Alamos National Laboratory, Los Alamos, New Mexico 87545, United States*

Kinga A. Unocic − *Center for Nanophase Materials Sciences, Oak Ridge National Laboratory, Oak Ridge, Tennessee 37830, United States*

Zhenglong Li − *Manufacturing Science Division, Oak Ridge National Laboratory, Oak Ridge, Tennessee 37830, United States*; orcid.org/0000-0001-8811-8625

Cameron M. Moore − *Chemistry Division, Los Alamos National Laboratory, Los Alamos, New Mexico 87545, United States*; orcid.org/0000-0001-7941-6591

Complete contact information is available at: https://pubs.acs.org/10.1021/acssuschemeng.4c01155

https://doi.org/10.1021/acssuschemeng.4c01155
ACS Sustainable Chem. Eng. XXXX, XXX, XXX−XXX

Notes

The authors declare the following competing financial interest(s): A.D. Sutton and M. J. Cordon have filed a patent application for the dioxolane-to-alkenes process discussed here.

■ ACKNOWLEDGMENTS

Microscopy research was sponsored by the U.S. Department of Energy (DOE), Office of Energy Efficiency and Renewable Energy, Bio-Energy Technologies Office, under contract DE-AC05-00OR22725 (ORNL) with UT-Battelle, LLC, and in collaboration with the Chemical Catalysis for Bioenergy (ChemCatBio) Consortium, a member of the Energy Materials Network. Microscopy and NH_3 TPD measurements were performed as part of a user project at the Center for Nanophase Materials Sciences (CNMS), which is a U.S. DOE Office of Science User Facility by the Scientific User Facilities Division, Office of Basic Energy Sciences, U.S. DOE. The authors thank Shawn K. Reeves for assistance with TEM sample preparation.

■ REFERENCES

(1) Eagan, N. M.; Kumbhalkar, M. D.; Buchanan, J. S.; Dumesic, J. A.; Huber, G. W. Chemistries and processes for the conversion of ethanol into middle-distillate fuels. *Nat. Rev. Chem.* **2019**, *3* (4), 223−249.

(2) Albright, L. F.; Marek, J. C. Mechanistic Model for Formation of Coke in Pyrolysis Units Producing Ethylene. *Ind. Eng. Chem. Res.* **1988**, *27* (5), 755−759.

(3) Li, F. W.; Li, Y. G. C.; Wang, Z. Y.; Li, J.; Nam, D. H.; Lum, Y.; Luo, M. C.; Wang, X.; Ozden, A.; Hung, S. F. Cooperative CO2-to-ethanol conversion via enriched intermediates at molecule-metal catalyst interfaces. *Nat. Catal.* **2020**, *3* (1), 75−82.

(4) Yang, S. H.; Mohagheghi, A.; Franden, M. A.; Chou, Y. C.; Chen, X. W.; Dowe, N.; Himmel, M. E.; Zhang, M. Metabolic engineering of Zymomonas mobilis for 2,3-butanediol production from lignocellulosic biomass sugars. *Biotechnol. Biofuels* **2016**, *9*, 15.

(5) Li, L. X.; Li, K.; Wang, K.; Chen, C.; Gao, C.; Ma, C. Q.; Xu, P. Efficient production of 2,3-butanediol from corn stover hydrolysate by using a thermophilic Bacillus licheniformis strain. *Bioresour. Technol.* **2014**, *170*, 256−261.

(6) Kubic, W. L.; Tan, E. C. D. Reactive Extraction Process for Separating 2,3-Butanediol from Fermentation Broth. *Ind. Eng. Chem. Res.* **2023**, *62* (12), 5241−5251.

(7) Davis, R.; Grundl, N.; Tao, L.; Biddy, M. J.; Tan, E. C. D.; Beckham, G. T.; Humbird, D.; Thompson, D. N.; Roni, M. S. *Process Design and Economics for the Conversion of Lignocellulosic Biomass to Hydrocarbon Fuels and Coproducts: 2018 Biochemical Design Case Update*; National Renewable Energy Laboratory, 2018.

(8) Affandy, M.; Zhu, C.; Swita, M.; Hofstad, B.; Cronin, D.; Elander, R.; Dagle, V. L. Production and catalytic upgrading of 2,3-butanediol fermentation broth into sustainable aviation fuel blendstock and fuel properties measurement. *Fuel* **2023**, *333*, 11.

(9) Adhikari, S. P.; Zhang, J. Y.; Guo, Q. Y.; Unocic, K. A.; Tao, L.; Li, Z. L. A hybrid pathway to biojet fuel via 2,3-butanediol. *Sustain. Energy Fuels* **2020**, *4* (8), 3904−3914.

(10) Nguyen, N. T. T.; Matei-Rutkovska, F.; Huchede, M.; Jaillardon, K.; Qingyi, G.; Michel, C.; Millet, J. M. M. Production of 1,3-butadiene in one step catalytic dehydration of 2,3-butanediol. *Catal. Today* **2019**, *323*, 62−68.

(11) Wu, J.; Peng, Z. M.; Sun, P. P.; Bell, A. T. n-Butane Dehydrogenation over Pt/Mg(In)(Al)O. *Appl. Catal. A-Gen.* **2014**, *470*, 208−214.

(12) Xie, S. Q.; Li, Z. X.; Zhu, G. D.; Song, W. L.; Yi, C. H. Cleaner production and downstream processing of bio-based 2,3-butane-diol: A review. *J. Clean Prod.* **2022**, *343*, 18.

(13) Priya, A.; Dureja, P.; Rathi, R.; Lal, B. Comparative assessment of separation techniques for downstream processing of 2,3-Butanediol. *Fuel* **2021**, *292*, No. 120351.

(14) Qureshi, N.; Meagher, M. M.; Hutkins, R. W. Recovery of 2,3-Butanediol by Vacuum Membrane Distillation. *Sep. Sci. Technol.* **1994**, *29* (13), 1733−1748.

(15) Garcia-Chavez, L. Y.; Shazad, M.; Schuur, B.; de Haan, A. B. (Liquid plus liquid) equilibrium data for the separation of 2,3-butanediol from aqueous streams using tetraoctyl ammonium 2-methyl-1-naphthoate. *J. Chem. Thermodyn.* **2012**, *55*, 85−91.

(16) Gilani, H. G.; Khiati, G.; Haghi, A. K. Liquid-liquid equilibria of (water+2,3-butanediol+2-ethyl-1-hexanol) at several temperatures. *Fluid Phase Equilib.* **2006**, *247* (1−2), 199−204.

(17) Harrison, K. W.; Harvey, B. G. High cetane renewable diesel fuels prepared from bio-based methyl ketones and diols. *Sustain. Energy Fuels* **2018**, *2* (2), 367−371.

(18) Broekhuis, R. R.; Lynn, S.; King, C. J. Recovery of Propylene-Glycol from Dilute Aqueous-Solutions via Reversible-Reaction with Aldehydes. *Ind. Eng. Chem. Res.* **1994**, *33* (12), 3230−3237.

(19) Wegenhart, B. L.; Abu-Omar, M. M. A Solvent-Free Method for Making Dioxolane and Dioxane from the Biorenewables Glycerol and Furfural Catalyzed by Oxorhenium(V) Oxazoline. *Inorg. Chem.* **2010**, *49* (11), 4741−4743.

(20) Sporing, J. D.; Wiesenthal, J.; Pfennig, V. S.; Gatgens, J.; Beydoun, K.; Bolm, C.; Klankermayer, J.; Rother, D. Effective Production of Selected Dioxolanes by Sequential Bio- and Chemo-catalysis Enabled by Adapted Solvent Switching. *ChemSusChem* **2023**, *169*, DOI: , Article; Early Access.

(21) Wuts, P. G. M.; Greene, T. W. *Greene's Protective Groups in Organic Synthesis*; John Wiley & Sons, Inc., 2007.

(22) Xu, L. Z.; Zhang, S. S.; Li, H. J.; Jiao, K. Studies on synthesis and biological activities of novel triazole compounds containing 1,3-dioxolane. *Chem. Res. Chin. Univ.* **2002**, *18* (3), 284−286.

(23) Szwajczak, E.; Sierka, E.; Ludynia, M. Potential Role of Low-Molecular-Weight Dioxolanes as Adjuvants for Glyphosate-Based Herbicides Using Photosystem II as an Early Post-Treatment Determinant. *Cells* **2023**, *12* (5), 19.

(24) Bruns, K.; Conrad, J.; Steigel, A. Stereochemistry of Cyclic-Compounds 0.1. Synthesis and Configurational Assignment of Diastereomeric 2,4-Dioxaspiro 5.5 Undec-8-enes. *Tetrahedron* **1979**, *35* (21), 2523−2530.

(25) Penczek, S.; Kubisa, P.; Matyjaszewski, K. Cationic Ring-Opening Polymerization of Heterocyclic Monomers. 1. Mechanisms. *Adv. Polym. Sci.* **1980**, *37*, 1−144.

(26) Qiu, H.; Yang, Z. N.; Köhler, M.; Ling, J.; Schacher, F. H. Synthesis and Solution Self-Assembly of Poly(1,3-dioxolane). *Macromolecules* **2019**, *52* (9), 3359−3366.

(27) Zaban, A.; Zinigrad, E.; Aurbach, D. Impedance spectroscopy of Li electrodes. 4. A general simple model of the Li-solution interphase in polar aprotic systems. *J. Phys. Chem.* **1996**, *100* (8), 3089−3101.

(28) Gao, Y.; Zhao, Y. M.; Li, Y. G. C.; Huang, Q. Q.; Mallouk, T. E.; Wang, D. H. Interfacial Chemistry Regulation via a Skin-Grafting Strategy Enables High-Performance Lithium-Metal Batteries. *J. Am. Chem. Soc.* **2017**, *139* (43), 15288−15291.

(29) Ando, K.; Takemasa, Y.; Tomioka, K.; Koga, K. Stereoselective Reactions 0.21. Asymmetric Alkylation of Alpha Alkyl Beta-Keto-Esters to Alpha,Alpha-Dialkyl Beta-Keto-Esters Having Either (R)-Chiral or (S)-Chiral Quaternary Center Depending on the Solvent System. *Tetrahedron* **1993**, *49* (8), 1579−1588.

(30) Martin, V.; Jadhav, S.; Egelund, P. H. G.; Liffert, R.; Castro, H. J.; Krüger, T.; Haselmann, K. F.; Le Quement, S. T.; Albericio, F.; Dettner, F. Harnessing polarity and viscosity to identify green binary solvent mixtures as viable alternatives to DMF in solid-phase peptide synthesis. *Green Chem.* **2021**, *23* (9), 3295−3311.

(31) Staples, O.; Moore, C.; Leal, J. H.; Semelsberger, T. A.; McEnally, C. S.; Pfefferle, L. D.; Sutton, A. D. A simple, solvent free method for transforming bio-derived aldehydes into cyclic acetals for renewable diesel fuels. *Sustain. Energy Fuels* **2018**, *2* (12), 2742−2746.

https://doi.org/10.1021/acssuschemeng.4c01155
ACS Sustainable Chem. Eng. XXXX, XXX, XXX−XXX

(32) Mota, C. J. A.; da Silva, C. X. A.; Rosenbach, N.; Costa, J.; da Silva, F. Glycerin Derivatives as Fuel Additives: The Addition of Glycerol/Acetone Ketal (Solketal) in Gasolines. *Energy Fuels* **2010**, *24* (4), 2733−2736.
(33) Rajale, T.; Yang, X. K.; Judge, E. J.; Moore, C. M.; Martinez, A.; Guo, M. F.; Ramasamy, K. K.; Elander, R.; Sutton, A. D. Separation, recovery and upgrading of 2,3-butanediol from fermentation broth. *Biofuels Bioprod. Biorefining* **2023**, *17* (4), 1003−1011.
(34) Cordon, M. J.; Zhang, J. Y.; Purdy, S. C.; Wegener, E. C.; Unocic, K. A.; Allard, L. F.; Zhou, M. X.; Assary, R. S.; Miller, J. T.; Krause, T. R.; et al. Selective Butene Formation in Direct Ethanol-to-C3+-Olefin Valorization over Zn-Y/Beta and Single-Atom Alloy Composite Catalysts Using In Situ-Generated Hydrogen. *ACS Catal.* **2021**, *11* (12), 7193−7209.
(35) Yu, Z. H.; Lu, X. B.; Xiong, J.; Ji, N. Transformation of Levulinic Acid to Valeric Biofuels: A Review on Heterogeneous Bifunctional Catalytic Systems. *ChemSusChem* **2019**, *12* (17), 3915−3930.
(36) Borges, M. E.; Díaz, L. Recent developments on heterogeneous catalysts for biodiesel production by oil esterification and transesterification reactions: A review. *Renew. Sust. Energy Rev.* **2012**, *16* (5), 2839−2849.
(37) Monteiro, R. R. C.; dos Santos, I. A.; Arcanjo, M. R. A.; Cavalcante, C. L.; de Luna, F. M. T.; Fernandez-Lafuente, R.; Vieira, R. S. Production of Jet Biofuels by Catalytic Hydroprocessing of Esters and Fatty Acids: A Review. *Catalysts* **2022**, *12* (2), 24.
(38) Boz, N.; Dogu, T.; Murtezaoglu, K.; Dogu, G. Effect of hydrogen ion-exchange capacity on activity of resin catalysts in tert-amyl-ethyl-ether synthesis. *Appl. Catal. A-Gen.* **2004**, *268* (1−2), 175−182.
(39) Gaspar, D. J.; Mueller, C. J.; McCormick, R. L.; Martin, J.; Som, S.; Magnotti, G. M.; Burton, J.; Vardon, D.; Dagle, V.; Alleman, T. L.; et al. *Top 13 Blendstocks Derived from Biomass for Mixing-Controlled Compression-Ignition (Diesel) Engines: Bioblendstocks with Potential for Decreased Emissions and Improved Operability*; PNNL-31421; United States, 2021. https://www.osti.gov/biblio/1806564, https://www.osti.gov/servlets/purl/1806564.
(40) Woolery, G. L.; Kuehl, G. H.; Timken, H. C.; Chester, A. W.; Vartuli, J. C. On the nature of framework Bronsted and Lewis acid sites in ZSM-5. *Zeolites* **1997**, *19* (4), 288−296.
(41) Kester, P. M.; Miller, J. T.; Gounder, R. Ammonia Titration Methods To Quantify Bronsted Acid Sites in Zeolites Substituted with Aluminum and Boron Heteroatoms. *Ind. Eng. Chem. Res.* **2018**, *57* (19), 6673−6683.
(42) Rodríguez-González, L.; Hermes, F.; Bertmer, M.; Rodríguez-Castellón, E.; Jiménez-López, A.; Simon, U. The acid properties of H-ZSM-5 as studied by NH3-TPD and 27Al-MAS-NMR spectroscopy. *Appl. Catal. A-Gen.* **2007**, *328* (2), 174−182.
(43) Di Iorio, J. R.; Bates, S. A.; Verma, A. A.; Delgass, W. N.; Ribeiro, F. H.; Miller, J. T.; Gounder, R. The Dynamic Nature of Bronsted Acid Sites in Cu-Zeolites During NOx Selective Catalytic Reduction: Quantification by Gas-Phase Ammonia Titration. *Top. Catal.* **2015**, *58* (7−9), 424−434.
(44) Gorte, R. J. Design Parameters for Temperature Programmed Desorption from Porous Catalysts. *J. Catal.* **1982**, *75* (1), 164−174.
(45) Demmin, R. A.; Gorte, R. J. Design Parameters for Temperature-Programmed Desorption from a Packed-Bed. *J. Catal.* **1984**, *90* (1), 32−39.
(46) Bravo-Suarez, J. J.; Subramaniam, B.; Chaudhari, R. V. Ultraviolet-Visible Spectroscopy and Temperature-Programmed Techniques as Tools for Structural Characterization of Cu in CuMgAlOx Mixed Metal Oxides. *J. Phys. Chem. C* **2012**, *116* (34), 18207−18221.
(47) Dagle, V. L.; Dagle, R. A.; Kovarik, L.; Baddour, F.; Habas, S. E.; Elander, R. Single-step Conversion of Methyl Ethyl Ketone to Olefins over ZnxZryOz Catalysts in Water. *ChemCatChem.* **2019**, *11* (15), 3393−3400.
(48) Sitthisa, S.; Sooknoi, T.; Ma, Y. G.; Balbuena, P. B.; Resasco, D. E. Kinetics and mechanism of hydrogenation of furfural on Cu/SiO2 catalysts. *J. Catal.* **2011**, *277* (1), 1−13.
(49) Pham, T. T.; Lobban, L. L.; Resasco, D. E.; Mallinson, R. G. Hydrogenation and Hydrodeoxygenation of 2-methyl-2-pentenal on supported metal catalysts. *J. Catal.* **2009**, *266* (1), 9−14.
(50) Cordon, M. J.; Zhang, J. Y.; Samad, N.; Harris, J. W.; Unocic, K. A.; Li, M. J.; Liu, D. X.; Li, Z. L. Ethanol Conversion to C4+Olefins over Bimetallic Copper- And Lanthanum-Containing Beta Zeolite Catalysts. *ACS Sustain. Chem. Eng.* **2022**, *10* (18), 5702−5707.
(51) Cordes, E. H.; Bull, H. G. Mechanism and Catalysis for Hydrolysis of Acetals, Ketals, and ortho-Esters. *Chem. Rev.* **1974**, *74* (5), 581−603.
(52) Nikitina, M. A.; Ivanova, I. I. Conversion of 2,3-Butanediol over Phosphate Catalysts. *ChemCatChem.* **2016**, *8* (7), 1346−1353.
(53) Zheng, Q. X.; Grossardt, J.; Almkhelfe, H.; Xu, J. Y.; Grady, B. P.; Douglas, J. T.; Amama, P. B.; Hohn, K. L. Study of mesoporous catalysts for conversion of 2,3-butanediol to butenes. *J. Catal.* **2017**, *354*, 182−196.
(54) Shwan, S.; Skoglundh, M.; Lundegaard, L. F.; Tiruvalam, R. R.; Janssens, T. V. W.; Carlsson, A.; Vennestrom, P. N. R. Solid-State Ion-Exchange of Copper into Zeolites Facilitated by Ammonia at Low Temperature. *ACS Catal.* **2015**, *5* (1), 16−19.
(55) Vandergrift, C. J. G.; Wielers, A. F. H.; Joghi, B. P. J.; Vanbeijnum, J.; Deboer, M.; Versluijshelder, M.; Geus, J. W. Effect of the Reduction Treatment on the Structure and Reactivity of Silica-Supported Copper Particles. *J. Catal.* **1991**, *131* (1), 178−189.
(56) Borodzinski, A.; Bonarowska, M. Relation between crystallite size and dispersion on supported metal catalysts. *Langmuir* **1997**, *13* (21), 5613−5620.

https://doi.org/10.1021/acssuschemeng.4c01155
ACS Sustainable Chem. Eng. XXXX, XXX, XXX−XXX